

Evolution of the force distributions in jammed packings of soft particles

Jens Boberski,^{1,*} M. Reza Shaebani,^{2,†} and Dietrich E. Wolf¹

¹*Computational Physics Group, University of Duisburg-Essen, D-47048 Duisburg, Germany*

²*Department of Theoretical Physics, Saarland University, D-66041 Saarbrücken, Germany*

(Dated: February 26, 2018)

The evolution of the force distributions during the isotropic compression of two dimensional packings of soft frictional particles is investigated numerically. Regardless of the applied deformation, the normal contact force distribution $P(f_n)$ can be fitted by the product of a power-law, and a stretched exponential, while the tangential force distribution $P(f_t)$ is fitted well by a Gaussian. With increasing strain, the asymptotic behavior at large forces does not change, but both $P(f_n)$ and $P(f_t)$ exhibit a broadening, even though, when scaled with the average forces, their widths decrease. Furthermore, the distribution of friction mobilization $P(\eta)$ is a decreasing function of $\eta = |f_t|/(\mu f_n)$, except for an increased probability of fully mobilized contacts ($\eta=1$). The excess coordination number of the packings increases with the applied strain, indicating that the more a packing is compressed the more stable it becomes.

PACS numbers: 45.70.Cc, 83.80.Fg, 61.43.-j, 81.05.Rm, 46.65.+g

I. INTRODUCTION

When subject to external forces, disordered materials such as emulsions, colloidal suspensions, and granular media exhibit a nontrivial response, which has received considerable attention over the last two decades [1, 2]. Highly heterogeneous force networks form between the particles [3, 4] and one of the main concerns regarding the contact force statistics is their asymptotic behavior at large forces.

Early experimental measurements [5–7] and numerical simulations with contact dynamics [8] or soft particle methods with Hookian [9, 10] and Hertzian [5, 10] interactions reported an exponential tail for the normal force distribution $P(f_n)$. However, faster than exponential tails were also found later in experiments [11–13] and simulations with Hookian [14], Hertzian [12, 14, 15] and other force laws [16, 17]. There have been theoretical attempts to explain the tail behavior [18] which mainly support the exponential decay. More recently, Tighe et al. [19] took the force balance at the particle level into account when maximizing the entropy with respect to the admissible force states and proposed an analytic expression for the normal force distribution in static granular media, predicting a Gaussian behavior for large forces, supported by a numerical study [20] within the framework of the force network ensemble [3, 21]. Some of the studies observe a crossover from an exponential-like to a faster than exponential behavior with increasing the applied isotropic compression [12, 14, 15, 22–24]. In this paper we provide numerical evidence for the faster than exponential decay in frictional soft spheres, and address the question whether the asymptotic behavior changes qualitatively when approaching the jamming transition.

Much less has been reported so far on the tangential force distribution $P(f_t)$ [8, 10, 11, 22, 25] and the evolution of the force distributions during deformation processes. Here, we study the evolution of the tangential force distribution as well as the friction mobilization during the isotropic compression. Note that for example the experiments on photoelastic particles provide evidence for a different behavior of the force distributions in sheared systems. For example, $P(f_n)$ of sheared packings decays much more slowly than that of the compressed ones. Besides the path dependence of the deformation, shear induced anisotropy has been also reported [11, 25]. The study of sheared systems is however beyond the scope of this work.

II. SIMULATION METHOD

In this report, the evolution of the inter-particle forces during a quasi-static isotropic compression was studied numerically (using DEM simulations). The two dimensional simulation box has periodic boundaries to avoid effects due to the presence of walls. The particle interactions are computed, using a linear spring-dashpot model for both normal and tangential forces (with the spring constant ratio k_t/k_n either being 0.5 or 1), as well as the Hertz-Mindlin model as described in [26]. The tangential force is additionally limited by the Coulomb limit. The results presented throughout the paper belong to the linear force law with friction coefficient $\mu=0.5$ and stiffness ratio $k_t/k_n=0.5$, unless stated otherwise.

The packings consist of nearly 14,200 disks with radii taken from a uniform distribution in the range $[0.8\bar{r}, 1.2\bar{r}]$, where \bar{r} is the average particle radius and is used as the natural unit of length in the following. The unit of force is chosen to be $k_n\bar{r}$.

The initial configuration is generated by randomly placing the particles without accepting any overlap between them. Afterwards, this unjammed system is com-

*Electronic address: jens.boberski@uni-due.de

†Electronic address: shaebani@lusi.uni-sb.de

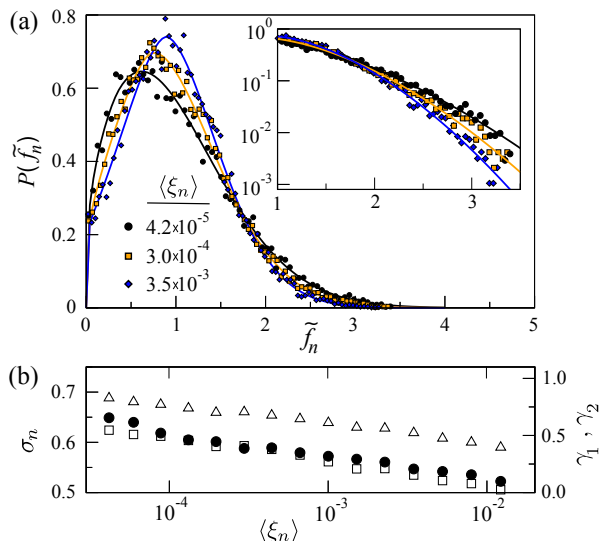


FIG. 1: (Color online) (a) Distribution of the normalized normal forces $\tilde{f}_n = f_n / \langle f_n \rangle$ for increasing applied deformation. Inset: the same plot in log-lin scale. The lines are fits using Eq. (1). (b) The standard deviation σ_n (full circles), the skewness γ_1 (open triangles), and the excess kurtosis γ_2 (open squares) versus $\langle \xi_n \rangle$.

pressed quasi-statically through a sequence of incremental compression and relaxation steps. A compression step is realized by re-scaling the particle positions and keeping their radii fixed. The relaxation routine ensures that the net force exerted on each particle is a factor of 10^{-8} below the mean contact force, before the next deformation step starts. Each time the system is equilibrated, the force state of the packing is stored. This process continues until the average overlap exceeds a given value. Upon decreasing the volume, the average overlap $\langle \xi_n \rangle$ remains zero until the jamming transition is reached. Beyond this transition $\langle \xi_n \rangle$ increases with the compression and, due to its purely geometric origin, is chosen as the order parameter to characterize the jammed state. Note that O’Hern et al. [14] suggested that averaging over configurations with slightly different average forces can distort the results close to the jamming transition. To avoid such effects, the calculated distributions in our study are taken from single realizations.

III. NUMERICAL RESULTS

A. Normal force distribution

Upon increasing the deformation in our simulations, not only the mean value of f_n increases but also the shape of the distribution is affected, e.g., the standard deviation and skewness change. Using the normalized contact force $\tilde{f}_n \equiv f_n / \langle f_n \rangle$, three typical distributions $P(\tilde{f}_n)$ at different values of $\langle \xi_n \rangle$ are shown in Fig. 1(a). In all cases, the distribution has a peak and one can see that the tail

of the distributions gradually becomes more bent during the compression process. These results, as well as the observations for the tangential forces and mobilization (discussed below) are in good agreement with experimental results by Majmudar and Behringer [11]. Fits of the form

$$P(\tilde{f}_n) = \frac{1}{N} (\tilde{f}_n)^{\nu_n} \exp\left(-\left|\frac{\tilde{f}_n - b_n}{w_n}\right|^{\delta_n}\right), \quad (1)$$

weighted with the reciprocal variance, are found to characterize the shape of $P(\tilde{f}_n)$ for different compressions (see lines in Fig. 1(a)). The fitting parameters N , ν_n , w_n , b_n , and δ_n are not independent, due to constraints for the normalization $\int_0^\infty P(\tilde{f}_n) d\tilde{f}_n = 1$ and on the first moment $\int_0^\infty \tilde{f}_n P(\tilde{f}_n) d\tilde{f}_n = 1$ of the distribution. Thus the number of fit parameters can be reduced to three. Even without taking the constraints into account during fitting, they are fulfilled with deviations below 0.5%.

Note that the fit in Eq. (1) captures not only the tail behavior but also the overall shape of the distribution with effectively three fitting parameters. The robustness of the results with respect to the microscopic properties of the interparticle force is studied, using different values of friction coefficient μ and stiffness ratio k_t/k_n , as well as linear and non-linear force laws. The results for four sets of the parameters are shown in Fig. 2. While the exact values of the fitting parameters depend on the contact force properties, the qualitative behavior in terms of the mean normal overlap is universal. For example, the exponent δ_n is found to be independent of the compression with values ranging from 1.65 to 1.8, depending on the contact properties. Allowing for this additional parameter leads to fits that capture the tail behavior substantially better than Gaussian ($\delta_n=2$) or exponential ($\delta_n=1$) fits. This supports the reports on a decay faster than exponential for large forces and shows that while the shape of the distribution changes as the jamming transition is approached, the asymptotic behavior for large forces remains the same.

The evolution of the width w_n with increasing deformation is shown in Fig. 2, indicating that the normalized distributions become narrower. The figure also shows that the exponent ν_n decreases with $\langle \xi_n \rangle$, while the shift b_n increases with the compression. In Fig. 1(b), the shape change of $P(\tilde{f}_n)$ is investigated by calculating higher moments of the force sets. The standard deviation, σ_n , of the data decreases with $\langle \xi_n \rangle$, similar to the behavior of w_n . A smaller standard deviation of the normalized forces at higher compression corresponds to a more homogeneous force network. For comparison, let us consider a situation where all contact forces are just rescaled, when increasing the external load. In this case, the relative width of the force distribution would remain constant. The fact that σ_n decreases may be attributed to the possibility of opening and closing of new contacts during the compression, and also to the nonaffine motions which allow local changes of the overlaps leading to a more uniform stress at large deformation.

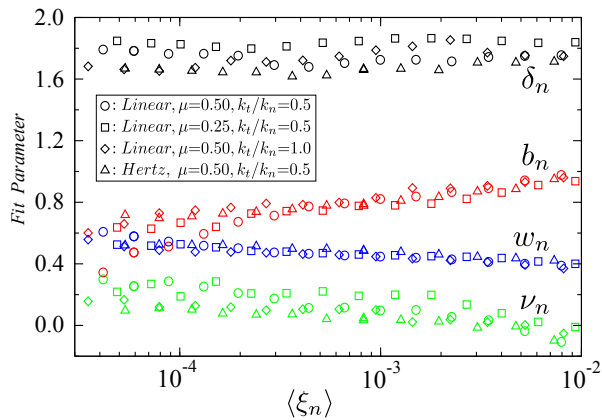


FIG. 2: (Color online) The compression dependence of the fitting parameters δ_n , b_n , w_n , and ν_n according to Eq. (1) for systems with different contact force properties.

The skewness γ_1 , which reflects the degree of asymmetry of a distribution (for $\gamma_1=0$ being symmetric) is shown in Fig. 1. It is a decreasing function of $\langle \xi_n \rangle$, thus, the distributions become more symmetric at larger deformations. The excess kurtosis γ_2 describes the peakedness and tail behavior of the distribution. A higher γ_2 represents a fatter tail (slower decay). Therefore, the decrease of γ_2 in Fig. 1(b) agrees with the observation that the bending of the tail increases, when the packing is more compressed. The behavior for γ_1 and γ_2 may have led to the impression of a crossover between an exponential and Gaussian tail in previous publications.

B. Tangential force distribution

The distribution of tangential forces is a monotonically decreasing function of f_t , without a notable peak or plateau. Figure 3(a) shows that the data nearly collapse for different compressions, if the forces are normalized with the mean force $\tilde{f}_t \equiv |f_t| / \langle |f_t| \rangle$, which means that the distribution broadens with increasing strain. The semi-logarithmic inset shows an increasing curvature with increasing average overlap (even though much less pronounced than for $P(\tilde{f}_n)$), indicating a non-exponential behavior. The data over the whole range of tangential forces can be fitted with

$$P(\tilde{f}_t) = \frac{1}{N} \exp \left[- \left(\frac{\tilde{f}_t}{w_t} - b_t \right)^2 \right], \quad (2)$$

where b_t is the fitting parameter and the normalization gives $N = \frac{1}{2} w_t \sqrt{\pi} (1 + \text{erf}(b_t))$, while the constraint for the first moment leads to

$$w_t = \frac{1 + \text{erf}(b_t)}{b_t + b_t \text{erf}(b_t) + \frac{1}{\sqrt{\pi}} \exp(-2b_t^2)}. \quad (3)$$

Adding a variable exponent (like δ_n in (1)) in the exponential function as an additional parameter does not

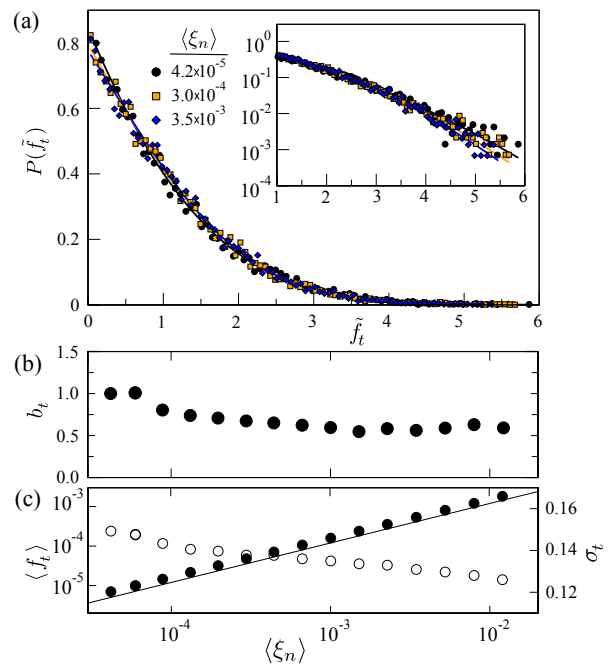


FIG. 3: (Color online) (a) Distribution of normalized tangential forces $P(\tilde{f}_t)$ for different values of the mean overlap $\langle \xi_n \rangle$. Inset: same in log-lin scale. The lines indicate fits given by Eq. (2). (b) The shift b_t of the Gaussian versus $\langle \xi_n \rangle$. (c) The average tangential force $\langle f_t \rangle$ (full circles) and the standard deviation σ_t (open circles) versus $\langle \xi_n \rangle$. The solid line corresponds to a linear increase.

improve the fit. Adding an additional power law term, leads to a small, negative exponent (~ -0.05) and thus an almost constant pre-factor. An alternative fit to an exponential which has been proposed in the literature is only applicable for the tail in the low deformation regime and can not be supported by the data in this study.

Figure 3(b) shows that b_t first decreases with compression and then reaches an overlap-independent regime for overlaps larger than 10^{-3} . The standard deviation σ_t of the normalized tangential forces, shown in figure 3(c), decreases by about 25% similarly to σ_n . The average tangential force increases linearly with increasing overlap (see Fig. 3(c)).

C. Friction mobilization

To elucidate the influence of friction on the evolution of the contact forces, the distribution of friction mobilization $P(\eta)$ is studied. The Coulomb condition specifies that $|f_t| \leq \mu f_n$. Therefore, the mobilization $\eta = |f_t| / \mu f_n$ quantifies the distance of a contact from the Coulomb friction limit. It varies within the range $[0, 1]$, with $\eta=1$ for fully mobilized contacts, i.e. those contacts in the static packing that are on the verge of sliding. Figure 4(a) shows that $P(\eta)$ decays with increasing η except for a peak at $\eta \approx 1$. Similar results were observed in experi-

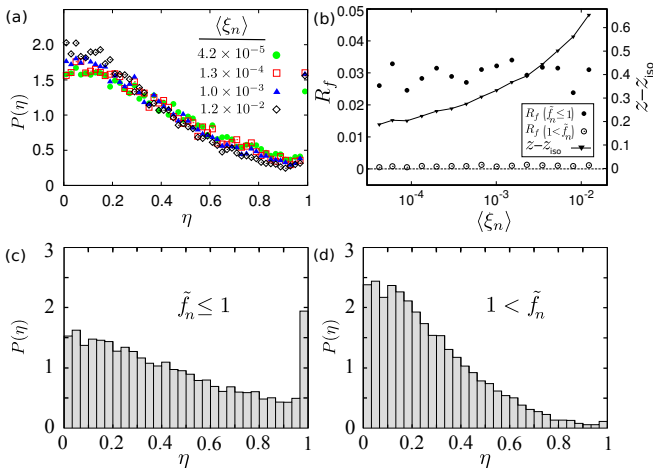


FIG. 4: (Color online) (a) Distribution of friction mobilization $P(\eta)$ for different strains. (b) Fraction of the nearly mobilized contacts R_f (separately shown for small and large normal forces), and the distance from isostaticity $z - z_{iso}$ in terms of $\langle \xi_n \rangle$ for the linear force law with $\mu = k_t/k_n = 0.5$. (c), (d) Histograms of the friction mobilization η for small and large forces in the packing with $\langle \xi_n \rangle = 1.2 \times 10^{-2}$.

ments with photoelastic particles [11]. The decay of $P(\eta)$ shows that most of the contacts are far from the Coulomb limit. With increasing deformation, $P(\eta)$ grows for small and decreases for large η , i.e. the probability distribution becomes steeper. The probability of fully mobilized contacts, however, remains approximately independent of $\langle \xi_n \rangle$. This is shown more clearly in Fig. 4(b), where the fraction R_f of contacts with a mobilization close to one ($\eta > 0.99$) is separately calculated for weak ($\tilde{f}_n \leq 1$) and strong ($1 < \tilde{f}_n$) normal forces, since the underlying mechanisms of stress propagation have been found to be different for these two subnetworks [27]. R_f fluctuates around 3% (0.1%) for weak (strong) forces. Note that these values depend in general on the friction coefficient [28]. The constant nature of R_f together with the increase of the average coordination number z with $\langle \xi_n \rangle$ indicates that the excess coordination number of the packing $\Delta z = z - z_{iso}$ grows when increasing the applied deformation [Fig. 4(b)]. It was shown that the mechanical response of frictional packings exhibits a critical scaling with Δz in the limit of $\Delta z \rightarrow 0$ [29]. More generally, Δz influences the extent of force indeterminacy which governs the stability of the granular packings [30]. The enhancement of mechanical stability with increasing the compression can be also traced back to the fact that topological properties of the force network, like the number of triangular structures, evolve during the process [31], allowing to predict the jamming transition point. The triangular structures are found to play an important role in stabilizing the packing [32].

The majority of the contacts with a mobilization close to 1 carry a normal force below the average. Figures 4(c) and (d) show the distribution of η separately for both

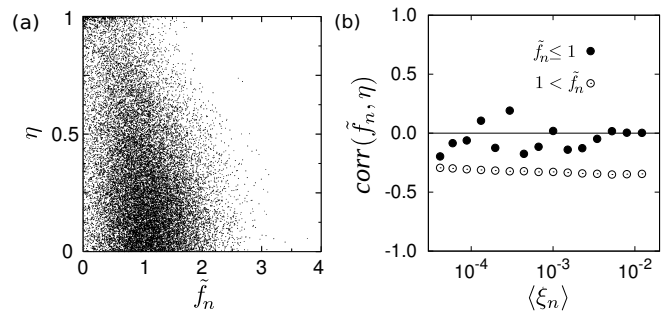


FIG. 5: (Color online) (a) A scatter plot of η versus \tilde{f}_n for the packing with $\langle \xi_n \rangle = 1.9 \times 10^{-3}$. (b) The correlation between \tilde{f}_n and η as a function of $\langle \xi_n \rangle$, separately shown for small (full circles) and large (open circles) forces.

categories of forces. In addition to the difference at $\eta \approx 1$, the histogram is steeper for strong forces. This shows that the force network of the strong forces is more stable and sliding events mainly occur at weak contacts.

The simulation results reveal a dependence of the friction mobilization at a contact on the magnitude of the normal force carried by that contact. Figure 5(a) shows a typical scatter plot of η versus \tilde{f}_n . The accumulation of contacts with $\eta = 1$ denotes the fully mobilized contacts at the edge of the Coulomb friction cone. For weak normal forces, the data points are scattered over the whole range of possible mobilizations. However, at strong normal forces, they tend towards smaller values of η and the fraction of fully mobilized contacts diminishes. This results in the decrease of the average mobilization as a function of the normal force (not shown). Thus the contacts which carry small normal forces are more liable for non-elastic deformations not only due to the higher chance of opening for such contacts (because of a smaller overlap), but also due to sliding, since these contacts have a larger mobilization. To quantify the relation, the Pearson correlation coefficient of \tilde{f}_n and η is shown in Fig. 5(b). The correlation is calculated for each packing, separately for weak and strong forces. While the correlations are scattered around zero for weak normal forces, there is a robust anti-correlation between \tilde{f}_n and η for strong forces, which remains unchanged over the whole range of deformations. This verifies again that \tilde{f}_n and η are inversely related to each other, and that larger forces show a lower probability to exceed the sliding threshold than small forces.

IV. CONCLUSIONS

The inter-particle force evolution during the isotropic compression of soft particle packings was investigated and empirical expressions for the normal and tangential force distributions were presented, that showed a faster than exponential decay for large forces. The results revealed that the relative width of the distributions de-

crease with increasing deformation, leading to a more homogeneous force network. It is notable that while the width of the distribution changes, the decay of the large forces remains unchanged. The investigation of friction mobilization η showed that, independent of the deformation, the fully mobilized contacts are most likely those carrying small normal forces. Finally, we note that the investigation of sheared systems is essential as a further step towards understanding the deformation at the microscopic level, which complements the theoretical studies based on the assumption of affine motion of particles [33] and facilitates the development of a general microscopic model for the deformation of granular materials.

Acknowledgments

We would like to thank Lothar Brendel for helpful discussions and carefully reading our manuscript. We would like to acknowledge the support by the German Research Foundation (DFG) via priority program SPP 1486 "Particles in Contact" and the Center for Computational Sciences and Simulation of the University of Duisburg-Essen.

-
- [1] R. M. Neddermann, *Statics and Kinematics of Granular Materials* (Cambridge University Press, Cambridge, 1992).
- [2] H. M. Jaeger, S. R. Nagel, and R. P. Behringer, *Rev. Mod. Phys.* **68**, 1259 (1996).
- [3] J. H. Snoeijer, T. J. H. Vlugt, M. van Hecke, and W. van Saarloos, *Phys. Rev. Lett.* **92**, 054302 (2004).
- [4] B. P. Tighe, J. E. S. Socolar, D. G. Schaeffer, W. G. Mitchener, and M. L. Huber, *Phys. Rev. E* **72**, 031306 (2005).
- [5] C. Liu, S. R. Nagel, D. A. Schecter, S. N. Coppersmith, S. Majumdar, O. Narayan, and T. A. Witten, *Science* **269**, 513 (1995).
- [6] J. M. Erikson, N. W. Mueggenburg, H. M. Jaeger, and S. R. Nagel, *Phys. Rev. E* **66**, 040301(R) (2002).
- [7] D. L. Blair, N. W. Mueggenburg, A. H. Marshall, H. M. Jaeger, S. R. Nagel, *Phys. Rev. E* **63**, 041304 (2001); G. Løvoll, K. J. Måløy, and E. G. Flekkøy, *Phys. Rev. E* **60**, 5872 (1999); D. M. Mueth, H. M. Jaeger, and S. R. Nagel, *Phys. Rev. E* **57**, 3164 (1998).
- [8] F. Radjai, M. Jean, J. J. Moreau, S. Roux, *Phys. Rev. Lett.* **77**, 274 (1996).
- [9] J. W. Landry, G. S. Grest, L. E. Silbert, and S. J. Plimpton, *Phys. Rev. E* **67**, 041303 (2003).
- [10] L. E. Silbert, G. S. Grest, and J. W. Landry, *Phys. Rev. E* **66**, 061303 (2002).
- [11] T. S. Majmudar and R. P. Behringer, *Nature* **435**, 1079 (2005).
- [12] H. A. Makse, D. L. Johnson, and L. M. Schwartz, *Phys. Rev. Lett.* **84**, 4160 (2000).
- [13] J. Zhou, S. Long, Q. Wang, and A. D. Dinsmore, *Science* **312**, 1631 (2006).
- [14] C. S. O'Hern, S. A. Langer, A. J. Liu, and S. R. Nagel, *Phys. Rev. Lett.* **88**, 075507 (2002).
- [15] H. P. Zhang and H. A. Makse, *Phys. Rev. E* **72**, 011301 (2005).
- [16] C. S. O'Hern, S. A. Langer, A. J. Liu, and S. R. Nagel, *Phys. Rev. Lett.* **86**, 111 (2001).
- [17] J. Brujic, S. F. Edwards, I. Hopkinson, and H. A. Makse, *Physica A* **327**, 201 (2003);
- [18] S. N. Coppersmith, C.-h. Liu, S. Majumdar, O. Narayan, T. A. Witten, *Phys. Rev. E* **53**, 4673 (1996); J. Rotter and M. O. Robbins, *Phys. Rev. Lett.* **89**, 195501 (2002); P. T. Metzger, *Phys. Rev. E* **70**, 051303 (2004); K. Bagi, *Granular Matter* **5**, 45 (2003); N. P. Krut' and L. Rothenburg, *Int. J. Solids Struct.* **39**, 571 (2002).
- [19] B. P. Tighe, A. R. T. van Eerd, and T. J. H. Vlugt, *Phys. Rev. Lett.* **100**, 238001 (2008).
- [20] A. R. T. vanEerd, W. G. Ellenbroek, M. vanHecke, J. H. Snoeijer, and T. J. H. Vlugt, *Phys. Rev. E* **75**, 060302(R) (2007).
- [21] J. N. Roux, *Phys. Rev. E* **61**, 6802 (2000); L. E. Silbert, D. Ertas, G. S. Grest, T. C. Halsey, D. Levine, *Phys. Rev. E* **65**, 031304 (2002); T. Unger, J. Kertesz, and D. E. Wolf, *Phys. Rev. Lett.* **94**, 178001 (2005); M. R. Shaebani, T. Unger, and J. Kertesz, *Phys. Rev. E* **79**, 052302 (2009).
- [22] R. C. Hidalgo, I. Zuriguel, D. Maza, I. Pagonabarraga, *Phys. Rev. Lett.* **103**, 118001 (2009).
- [23] D. Howell, R. P. Behringer, and C. Veje, *Phys. Rev. Lett.* **82**, 5241 (1999).
- [24] M. L. Nguyen and S. N. Coppersmith, *Phys. Rev. E* **62**, 5248 (2000).
- [25] J. Zhang, T. S. Majmudar, M. Sperl and R. P. Behringer, *Soft Matter* **6**, 2982 (2010).
- [26] L. E. Silbert, D. Ertas, G. S. Grest, T. C. Halsey, D. Levine, S. J. Plimpton, *Phys. Rev. E* **64**, 051302 (2001).
- [27] F. Radjai, D. E. Wolf, M. Jean, and J.-J. Moreau, *Phys. Rev. Lett.* **80**, 61 (1998).
- [28] K. Shundyak, M. van Hecke, and W. van Saarloos, *Phys. Rev. E* **75**, 010301(R) (2007).
- [29] E. Somfai, M. van Hecke, W. G. Ellenbroek, K. Shundyak, and W. van Saarloos, *Phys. Rev. E* **75**, 020301(R) (2007).
- [30] M. R. Shaebani, T. Unger, and J. Kertesz, *Phys. Rev. E* **76**, 030301(R) (2007); *Phys. Rev. E* **78**, 011308 (2008); J. H. Snoeijer, W. G. Ellenbroek, T. J. H. Vlugt, and M. van Hecke, *Phys. Rev. Lett.* **96**, 098001 (2006).
- [31] R. Arévalo, I. Zuriguel, and D. Maza, *Phys. Rev. E* **81**, 041302 (2010).
- [32] A. Tordesillas, D. M. Walker, and Q. Lin, *Phys. Rev. E* **81**, 011302 (2010).
- [33] M. R. Shaebani, J. Boberski, and D. E. Wolf, *Granular Matter* **14**, 265 (2012).